Non-invasive High-Intensity Focused Ultrasound Treatment of Liver Tissues in an In Vivo Porcine Model: Fast, Large and Safe Ablations Using a Toroidal Transducer

Sophie Cambronero, Aurélien Dupré, Charles Mastier, David Melodelima

Noninvasive treatment of liver tissues in an *in vivo* porcine model: fast, large and safe ablations using a toroidal transducer.

Sophie Cambronero[1], Aurélien Dupré[1,2], Charles Mastier[2], David Melodelima[1]

LabTAU, INSERM, Centre Léon Bérard, Université Lyon 1, Univ Lyon, F-69003, LYON, France

Centre Léon Bérard, Lyon, F-69008, LYON

Corresponding author:

Sophie CAMBRONERO

LabTAU

151 cours Albert Thomas

69424 Lyon Cedex 03

France

sophie.cambronero@gmail.com

ABSTRACT

A toroidal high-intensity focused ultrasound (HIFU) transducer was used to noninvasively treat liver tissues *in vivo* in a pig model. The transducer was divided into 32 concentric rings with equal surface areas operating at 2.5 MHz. First, attenuation of skin, fat, muscle and liver tissues was measured in fresh animal samples to adjust the energy delivered to the focal zone. Then, 8 animals were included in the present protocol and placed in a dorsal decubitus proclive position at an angle of 15°. The device was held by hand, and sonications were performed during apnea. Two thermal HIFU lesions were created in 40 s in each animal. The average abdominal wall thickness was 14.8 ± 1.3 mm (12.5-17.6). The longest and shortest axes of the HIFU ablations were 20.9 ± 6.3 mm (14.0–33.7) and 14.2 ± 5.5 mm (7.0–22.0), respectively. All HIFU lesions were visible on sonograms. The correlation between the dimensions of the HIFU lesions observed on sonograms and during gross examination was r = 0.84. Creating large and fast ablations with reliable ultrasound imaging guidance in the liver using this handheld device may represent a new therapeutic option for patients with liver tumors.

Keywords: HIFU, ultrasound, toroidal, noninvasive, liver, *in vivo*.

INTRODUCTION

Effective curative intent treatments of liver tumors is a major health issue (Bray, et al. 2018). Two forms of malignant liver tumors exist: (i) primary hepatic cancer, mainly hepatocarcinoma (HCC) (comprising 75%-85% of cases) and intrahepatic cholangiocarcinoma (10%-15%), and (ii) liver metastases. HCC usually develops on hepatic tissue affected by chronic inflammation, with 906,000 estimated new cases in 2020 worldwide (Sung, et al. 2021). Based on the patient's health condition, therapy mainly consists of surgery (resection or liver transplantation) or radiofrequency ablation (RFA). This minimally invasive technique emerged as a less aggressive alternative to surgery, especially for patients with comorbidities or impaired liver function. However, to date, only approximately 25% of patients are considered suitable candidates for curative treatment.

Liver metastases are another form of liver tumor and are often a consequence of colorectal cancer. Colorectal cancer ranks third in incidence among cancers in the world, with more than 1.9 million and 935,000 estimated new cases and deaths, respectively, in 2020 (Sung, et al. 2021). Approximately 50% of these patients are likely to develop liver metastases. To date, the only treatment with curative intent and long term survival is surgery with a five-year survival rate of approximately 50% (Nordlinger, et al. 2013, Evrard, et al. 2018). However, less than 20% of diagnosed patients are eligible for surgery. Patients are only eligible if complete resection of the colorectal liver metastases with clear margins is possible and if the remaining hepatic parenchyma is sufficient to provide postoperative liver functions (Nordlinger, et al. 2013). As a consequence, the size, number and/or location of the metastases can be an exclusion criterion for surgery.

High-intensity focused ultrasound (HIFU) is a worldwide therapeutic reality in a large variety of medical applications, including oncology (Kennedy 2005, Melodelima, et al. 2008,

Maloney and Hwang 2015, Bai, et al. 2016, Crouzet, et al. 2017, Lang and Wu 2017, Dupre, et al. 2019). However, despite this method's clinical potential, the liver is a particularly challenging organ for HIFU treatment due to the combined effect of respiratory-induced liver motion, partial blocking by the rib cage, and high perfusion/flow (Aubry, et al. 2013, N'djin, et al. 2015, Lesser, et al. 2016). Moreover, before reaching their target in the liver, the ultrasound waves will have to propagate through skin, fat and muscle layers. These tissues have different acoustic properties, such as density, speed of sound, and attenuation, that alter the focusing effect and energy deposition at the focus (Jung, et al. 2011). For example, skin or subcutaneous burns, either benign or severe (grade 3) needing surgical intervention, have been frequently (15%) reported in clinical studies (Sehmbi, et al. 2021) and represent the most common side effect of HIFU liver treatments. Another limitation of HIFU treatments is that the ablations are typically cigar-shaped with dimensions on the order of 8-15 mm (along the beam axis) x 1-3 mm (transverse to the beam axis) (Haar and Coussios 2007). As a consequence, the clinical treatment of solid tumors requires mechanical motion of the transducer to juxtapose hundreds of single spherical ablations until the entire tumor volume is covered. Such a procedure requires long treatment times and the implementation of an elaborate robotized arm combined with complex electronics (Kennedy, et al. 2004).

We have shown at the early clinical stage that a new form of treatment using toroidal HIFU transducers can be a promising tool for treating liver metastases (Dupre, et al. 2015). Before developing sophisticated devices, a first prototype was built to be used intraoperatively (during surgery) (Melodelima, et al. 2009, Parmentier, et al. 2009). This toroidal HIFU transducer achieved a fast, selective, safe and well-tolerated large volume of liver ablation (the ablation rate is more than 30 times faster than any other local therapy) without requiring puncture into the organ (N'djin, et al. 2010, Dupre, et al. 2017, Battais, et al. 2020). To date, 30 patients have been included in a phase I-II clinical trial using this device.

Thanks to this initial experience, we now aim to move forward with a completely noninvasive HIFU treatment in the liver for treating primary and secondary tumors. The first step described in this study was to use electronic focusing to place the focal zone deeply in liver tissues and to consider the differential attenuation induced by the intervening tissues by measuring the attenuation values in fresh animal samples. An *in vivo* study was then conducted in a porcine model to evaluate whether such a transducer can be used noninvasively by holding the device by hand, considering the specific thickness of each intervening tissue (skin, fat, muscle and liver tissues) before the focal zone to deliver the proper energy in under 40 s. The aim of this work was to evaluate the safety, tolerance and efficacy of a noninvasive HIFU procedure in an *in vivo* porcine model using a toroidal transducer.

MATERIALS AND METHODS

HIFU device

The toroidal HIFU device, which has been already described in previous publications (Caloone, et al. 2015, Cilleros, et al. 2021), has an active diameter of 67 mm and a radius of curvature of 70 mm. The transducer was divided into 32 concentric ring-shaped emitters with identical surface areas (78 mm^2), all operating at 2.5 MHz (Figure 1C). Due to the toroidal geometry, the focal zone is a ring of 30 mm in diameter at a depth of 70 mm. Moreover, due to the geometrical characteristics of a torus, the ultrasound beams coming from each of the 32 emitters intersect between the transducer and the focal ring to form a secondary focal zone (Figure 1A). The pressure in this additional focal zone is higher than the pressure in the focal ring as shown in Figure 1B ; this zone was therefore used to create large ablations (Battais, et al. 2020).

A sectorial ultrasound imaging probe working at a frequency of 7.5 MHz (Vermon, Tours, France) was placed at the center of the HIFU transducer and connected to an ultrasound scanner (EB4012, B-K Medical, Herlev, Denmark) to guide the treatment. The ultrasound imaging plane was aligned with the HIFU acoustic axis. Both transducers were placed into acoustic contact with the skin using sterile coupling water (Baxter, Deerfield, USA) contained in a polyurethane coating (CIV-Flex Transducer cover, CIVCO, Kalona, IA, USA). This coating attenuated the ultrasound pressure by approximately 2% at 2.5 MHz. To prevent the transducer from becoming too hot during the HIFU procedure, the water was cooled at 6 °C and flowed at a continuous rate of 0.6 L/min using a peristatic pump (Masterflex L/S Model 7555–05, Cole-Parmer Instruments Co., Chicago, IL, USA) in a closed cooling circuit. A 14 MHz ultrasound imaging probe (I14C5I, BK Medical, Herlev, Denmark) was used to obtain images with higher resolution.

The HIFU transducer-driving equipment was similar to that previously reported (Battais, et al. 2020). The amplifier (Image Guided Therapy, Pessac, France) has 32 channels programmable in phase and power. The phase of each channel could be adjusted with a resolution of 1 degree. The electrical power delivered by each channel could be adjusted up to 15 watts. The time needed to change the phase and/or power delivered was 1 ms. The spatial repartition and intensity of the pressure field produced can be controlled electronically by modulating the amplitude and the phase applied to each of the 32 individual transducers. The phase, emitted power and reflected power of each channel were analyzed and registered during the HIFU sonications thanks to a custom-made user interface. This interface also displayed the position of the HIFU focal region superimposed on the sonogram, making it possible to place the HIFU ablation in the tissues and visualize the treated zone immediately after each sonication.

Preparation of the animals and anesthesia

All procedures described in this paper were carried out in the Laboratory of Experimental Surgery (DSV 693880501). The animal experiments were performed under an institutional research protocol (PRO105) approved by the local ethical committee of animal experimentation. These experiments were conducted in accordance with the European legislation covering the use of animals for scientific purposes (Directive 2010/63/EU).

The experiments were conducted on eight Landrace pigs, 10-15 weeks old, weighing between 28 and 39 kg. A porcine model was specifically chosen because its anatomy and physiology are very close to those of humans. The animals were kept on-site 7 days before the start of the experiments and were fasted 24 h before the HIFU procedure. Premedication was achieved using an intramuscular injection of a mix of ketamine (15 $mg.kg^{-1}$), azaperone (2.2 $mg.kg^{-1}$) and atropine (0.5 mg) 15 minutes before anesthesia. A 20-gauge catheter was then placed in an auricular vein to induce and maintain anesthesia using Diprivan (Propofol 10 mg/mL). The animal was intubated and placed under assisted ventilation. Oxygenation was supplied by an assisted ventilation system (ABT 4300, Kontron Instruments) at a rate of 7.2 $l.min^{-1}$ and a frequency of 12 $cycles.min^{-1}$ (duty cycle: 40%). Blood oxygen saturation was monitored by an optical captor and maintained at 100%. Hydration was provided by isotonic perfusion of a physiological salt solution at 9%. The animals were positioned in a dorsal decubitus proclive position with an angle of 15°. This specific positioning allows to partially to move the liver below the rib cage in order to have an anatomical access to approximately 60% of the liver while avoiding the rib cage. The skin of the animals was shaved and washed on the abdomen at the site of the HIFU treatment.

The 14 MHz ultrasound imaging probe was used to image the region of the liver to be targeted and measured as precisely as possible the thickness of all tissues between the probe and the focus, including the thickness of the skin, fat and muscle layers. The position of the

ultrasound imaging probe was identified on the skin of the pig using a surgical pen. Using this landmark, the HIFU probe was then placed on the skin of the animal such that the imaging plane of the ultrasound imaging probe integrated with the HIFU transducer was aligned with the image obtained with the 14 MHz ultrasound imaging probe. The HIFU device was hand-held (Figure 2). A thin layer of degassed and demineralized water was applied to the HIFU window to establish acoustic coupling with the skin. Two target areas were identified in each animal. The targets had to be separated by at least 2 cm and, ideally in different lobes, in order to clearly identify each individual HIFU lesion. If possible, each ablation had to be performed at distance (at least 5 mm) from specific structures (gall bladder, the hepatic pedicle, and the vena cava) and aimed at liver tissues having thicknesses of at least 3 cm.

Treatment parameters

Preliminary to animal experiments, the attenuation coefficients of the porcine abdominal wall layers (i.e., skin, fat and muscle) and liver tissues were measured using the pulse-echo method (Barrere, et al. 2021, Sanchez, et al. 2021). Nine samples were recovered from pigs included in another protocol. Analyses were performed on fresh *ex vivo* samples. Samples were degassed before experiments (25 min at -0.8 bar) approximately 4h after the sampling. Before the samples were recovered, ultrasound images of the abdominal wall were also acquired at two distinct areas considered suitable for HIFU treatment, resulting in 18 acquisitions. For each image, the total abdominal wall length, as well as the skin, fat and muscle layer thicknesses were measured. Attenuation measurements were performed as described previously (Sanchez, et al. 2021). Briefly, the attenuation coefficients $\alpha(f)$, in $dB.cm^{-1}$, were calculated by performing the Fourier transform of the radio-frequency signals obtained from a plane reflector with and without the sample in the path between a pulse-echo

transducer working at 2.5 MHz and the reflector. Then, the log difference between the spectra was calculated using Equation 1:

$$\alpha_T(f) = \frac{20}{2d_T} \times \log\left(\frac{A_w(f)}{A_T(f)}\right) \qquad \text{Equation 1}$$

where $A_w(f)$ is the reference magnitude spectrum at frequency f, $A_T(f)$ is the tissue sample magnitude spectrum at frequency f, and d_T is the thickness of the tissue sample. The attenuation coefficient of the water was considered to be zero. The attenuation coefficients varied with the frequency, as described in Equation 2:

$$\alpha(f) = af^b \qquad \text{Equation 2}$$

where coefficient a was measured in dB.cm^{-1}.MHz^{-1}, f is the frequency in MHz, and coefficient b is dimensionless. The best-fit power-law method was used to determine coefficients a and b from the plots of the attenuation coefficients vs. frequency. The goodness-of-fit value according to the best-fit power law was determined using the R^2 value.

The speed of sound and the density of each sample were also measured and are presented in Table 2. The transmission coefficients for the water/skin, skin/fat, fat/muscle and muscle/liver interfaces were calculated (Table 2). The total transmission coefficient T was defined as the product of all the transmission coefficients listed in Table 2.

The attenuation in the prefocal tissues was computed using Equation 3:

$$\alpha(z_s, z_f, z_m, z_l) = \alpha_s z_s + \alpha_f z_f + \alpha_m z_m + \alpha_l z_l \qquad \text{Equation 3}$$

where α_s , α_f , α_m and α_l are the measured attenuations (dB.cm^{-1}) of the skin, fat, muscle and liver respectively, z_s , z_f , and z_m are the thicknesses (cm) of the skin, fat and muscle respectively, and finally z_l is the thickness of the liver from the muscle to the focus measured before each sonication (cm). The attenuation coefficients were adjusted to 2.5 MHz using Equation 2.

The applied power P_a was calculated from the measured electrical power during each sonication and the efficiency of the transducer (60%). The delivered power P_d was then calculated using Equation 4 by considering the attenuation in the prefocal tissues and the total transmission coefficient T=0.96:

$$P_d = P_a . T . 10^{-\frac{\alpha(z_S, z_f, z_m, z_l)}{10\ dB}} \qquad \text{Equation 4}$$

The acoustic energy after attenuation will be referred to as the delivered energy E_d and was computed from the delivered acoustic power P_d and the sonication time t (Equation 5):

$$E_d = P_d \times t \qquad \text{Equation 5}$$

The device used in this work was initially designed for intraoperative use (Melodelima, et al. 2007, Dupre, et al. 2017). The exposure parameters were adapted for noninvasive use based on numerical simulations that used the measured porcine attenuation values and measured tissue thickness as described above. The numerical modeling of HIFU treatments was similar to that described in previous studies (N'djin, et al. 2015). Here, each layer of tissue was represented by a rectangular parallelepiped. The attenuation, density and speed of sound of each tissue layer were obtained from ex vivo measurements as described above and are reported in Table 1. Liver perfusion was set to 30 kg.m-3.s-1 (N'djin, et al. 2015). The blood vessel network was not modeled. An acoustic power of 115W was identified as sufficient for the creation of HIFU ablations in homogeneous perfused liver tissues. All HIFU sonication procedures were performed with two consecutive exposures of 20 s each. In each sonication, the second focal zone was used to create the ablations. The depth and diameter of the focal ring changes the position and size of the second focal zone (Figure 1A). First, the depth of the ring-shaped focus was set electronically at 68 mm, and its radius was set at 2 mm. Under these settings, the maximum pressure zone was located 36 mm below the skin (i.e., approximately 21 mm deep in the liver tissues depending on the thickness

of the intermediate tissues). Without moving the HIFU device and without any delay, a second sonication was performed by electronically setting the depth of the ring-shaped focus at 66 mm and its radius at 1 mm. Under these settings, the secondary focal zone was located 34 mm deep below the skin (i.e., approximately 19 mm deep in liver tissues depending on the thickness of the intermediate tissues). In the first two animals, noninvasive HIFU ablations were created using an applied acoustic power set to 115 W corresponding to an energy of 4.6 kJ. The other six animals were treated using an applied acoustic power set to 140 W corresponding to an energy of 5.6 kJ for adjusting to *in vivo* perfusion. The treatment parameters are summarized in Table 1.

HIFU procedure

Two HIFU ablations were created in the liver, at distinct locations, in each animal. Each HIFU sonication was performed during apnea to avoid liver movement. After inhalation, the apnea periods began between 5 and 20 s before sonication and lasted at most 60 s. The oxygenation of the animals was controlled during treatment to preserve a minimal blood oxygen saturation of 80%. When the treatment was completed, all of the lesions were observed and measured on the sonograms using the 7.5 MHz ultrasound imaging probe located in the center of the device. The 14 MHz ultrasound imaging probe was also used to observe the lesions with higher resolution. The longest and shortest axes of the treated area visible on the sonograms were measured. The skin was examined for any macroscopic signs of damage.

After the treatment, the animals were returned to their pens and observed twice daily for signs of anorexia, distress, fever and general behavior. Seven days after the HIFU treatment, the animals were anesthetized using the same procedure described above. The HIFU lesions were imaged using the 14 MHz ultrasound imaging probe placed on the skin of

the animals. A laparotomy was then performed to examine the liver and adjacent organs for any macroscopic signs of damage. Analgesia (Sufenta 150 µg/5mL) was injected once on the first 6 animals (3mL/h) during the surgical procedure. Additional ultrasound images of the HIFU lesions were acquired intraoperatively using the 14 MHz ultrasound imaging probe. The animals were then euthanized by an injection of pentobarbital (182 mg/mL) before removing the liver. The treated zones of the liver were sliced along a plane passing through the middle of the HIFU lesion and perpendicular to the sample's surface. HIFU ablations were then classified into 3 categories: absence of ablation (NT: Not Treated), non-compliant (TNC: Treated but Non-Compliant), and compliant (T: Treated). The compliance was assessed based on the ablation shape and size. The expected ablation shape was a homogeneous truncated cone as observed in previous work using the same device intra-operatively (Melodelima, et al. 2009). The expected ablation size, estimated via numerical simulations, were at least 10 mm in width by 15 mm in length. The samples were then analyzed for gross examination (see Data analysis) and then fixed in a 4% solution of formaldehyde. After 48 h, the samples were transferred to phosphate-buffered saline and then dehydrated using increasing concentrations of alcohol, treated with intermedium and embedded in paraffin. The embedded samples were sliced and stained using hematoxylin and eosin. The tissues were examined with a brightfield microscope.

Data analysis

Each sample was placed on an even surface containing a reference scale, and a photograph was taken to generate a near isometric view of the sample. Images of the lesions were then analyzed using the Measure tool of ImageJ, version 1.52a (National Institutes of Health, USA; http://imagej.nih.gov/ij). The longest and shortest axes of the treated area

visible as a white necrotic core on the tissue sample surface were measured. All measured data are given as the mean values ± standard deviations (minimum value - maximum value).

RESULTS

Attenuation measurements

On average, the abdominal wall thickness (including the skin, fat and muscle layers) was 14.8 ± 1.3 mm (12.5-17.6). The thicknesses of the skin, fat and muscle layers averaged 2.3 ± 1.1 mm, 8.4 ± 2.8 mm and 4.7 ± 0.8 mm, respectively. The averages of coefficients *a* and *b* in the skin, fat, muscle and liver tissues are summarized in Table 2.

Overview of the HIFU treatments

The animals tolerated the treatment well over the experimental period. The animals remained hemodynamically stable during the procedure. They recovered from the procedure within 2 h after termination of anesthesia and quickly resumed eating and normal behavior with no signs of pain or fever. The mean weight gain was normal (1.9 ± 0.5 kg) based on the age of the animals.

Table 1 shows an overview of the treatment parameters. Twelve out of the sixteen HIFU sonications resulted in visible damage at the target site. Two HIFU exposures did not result in visible damage due to insufficient delivered energy at the targeted site. Two HIFU exposures resulted in gastric damage (not shown or included in Table 1). In these two cases, the liver thickness was smaller than the longest axis of the lesion. Three sonications led to HIFU lesions at the target whose sizes were not compliant with the desired lesion size. Once sufficient energy was delivered to the homogeneous parenchyma at the target site, nine HIFU sonications led to visible liver damage (macroscopically, microscopically and on the ultrasound images) compliant with the desired lesion size.

Analysis of sublethal sonications and noncompliant HIFU lesions

The first two HIFU sonications were performed using an applied acoustic power of 115 W, which was not sufficient for creating an ablation. Based on the numerical simulations, this value was estimated as the minimal acoustic power required for treatment. All other HIFU sonications were performed using an applied acoustic power of 140 W, the highest value deliverable while avoiding secondary lesions in the intervening tissues. Three HIFU sonications (n=3, 5 and 8) were created around large blood vessels that measured at least 8 mm in diameter (Figure 3). No thrombosis was observed in these vessels. However, the HIFU ablations were affected by the heat-sink effect of the blood flow. The applied energy for these sonications was between 1920 and 2112 J; i.e. above the threshold (1882 J) needed for the creation of an ablation in homogeneous liver parenchyma, suggesting that higher energy is required close to large blood vessels.

Analysis of compliant ablations

Figure 4 shows three typical HIFU ablations (n=10, 12 and 13) created noninvasively in the liver in 40 seconds, even around small blood vessels (diameter < 5 mm). The coagulated tissues are clearly distinguishable from the untreated tissues. The treated region appears as an off-white color, which is sometimes darker at the most heated points. Considering all compliant HIFU ablations, the abdominal wall thickness was on average 15.4 ± 2.9 mm. The longest and shortest axes of the HIFU ablations were 20.9 ± 6.3 mm (14.0–33.7) and 14.2 ± 5.5 mm (7.0–22.0), respectively. These HIFU ablations were performed at an average depth (distance from the skin to the beginning of the HIFU ablations) of 19.2 ± 4.2 mm while preserving the integrity of the skin and intervening tissues.

Homogeneous coagulation necrosis was confirmed by histological analysis. A typical example of the histological analysis is given in Figure 5 corresponding to HIFU ablation

number 9. The HIFU treatments did not affect the animals' well-being and were well tolerated. If the treatment time is 40 s, a delivered energy of approximately 1900 J (i.e., a delivered acoustic power of approximately 50 W) is required to create an ablation in the liver. The HIFU ablations were visible with high contrast in the ultrasound images. Figure 6 shows the typical ultrasound images that were acquired at D0 before (Fig. 6a) and after the HIFU sonications (Fig. 6b) and at D7 before (Fig. 6c) and after (Fig. 6d) laparotomy. A hyperechoic zone was visible at the location of the maximal pressure deposition a few minutes after HIFU sonication (Figure 6b). This hyperechoic zone was surrounded by a hypoechoic region. These observations were still found at D7 either on transcutaneous or intraoperative ultrasound imaging examination (Figure 6c and 6d). At Day 7, a hyperechoic boundary was also observed all around the ablation intraoperatively. In all cases, a strong correlation was found between the dimensions measured on ultrasound images and the dimensions measured macroscopically using intraoperative ($r = 0.96$, $p < 0.05$) or transcutaneous ($r = 0.84$, $p < 0.05$) measurements (Figure 7).

DISCUSSION

This study was designed to confirm the feasibility, safety, and efficacy of noninvasive HIFU ablation of the liver parenchyma using the same HIFU toroidal transducer used intraoperatively in humans for the treatment of liver metastases (Dupre, et al. 2015, 2019). Treatments with proper electronic focusing and energy adjustment regarding attenuation allowed for the determination of sonication parameters to create safe thermal ablations measuring on average 21 mm long by 14 mm wide. The HIFU sonications were completed in 40 seconds. All treatments were well tolerated and did not affect the animals' well-being. The energy delivery threshold for compliant ablations under such treatment conditions was found

to be greater than or equal to 1882 J at the focus in homogeneous liver parenchyma. Such energy also allowed the creation of homogeneous ablations around blood vessels of up to 5 mm in diameter.

When blood vessels of more than 8 mm in diameter were present in the treatment zone, even a delivered energy of approximately 2200 J was not sufficient to create a compliant ablation due to the effect of the heat-sink effect of the blood flow. Treatment parameters should then be adjusted when ablating around large blood vessels. In this study, the numerical model estimated only the ablation in homogenous liver tissues (i.e. without large vessels at the focal zone). Indeed, a more realistic simulation including real-time, 3D modeling of large blood vessels (>5 mm in diameter) and their complex architecture could refine simulation outcomes aimed at improving personalized treatment. In previous studies, we demonstrated that homogeneous ablations can be performed around large blood vessels (from 5 to 10 mm in diameter) using the same device if the delivered energy was approximately 17 kJ (Cambronero, et al. 2020). The information presented in Table 1, and this study in general, highlights the importance of taking attenuation into account and adjusting the delivered energy to the tissue to spare the intermediate tissues, thus suggesting that HIFU treatments should be personalized for each patient.

At present, HIFU treatments are either guided by ultrasound imaging or magnetic resonance imaging (MRI). MRI-guided devices use MR-thermometry to measure the tissue response with a spatial resolution on the order of one millimeter and a temperature resolution of less than 1 degree Celsius (Melodelima, et al. 2005, De Senneville, et al. 2016, Siedek, et al. 2019). Therefore, MRI offers good clarity in three-dimensional imaging but it has a high cost, especially for lengthy procedures, and it has low spatial and temporal resolution when compared with ultrasound imaging. Ultrasound-guided devices use diagnostic ultrasound probes both to locate the target and to observe the response. Non-invasive HIFU treatments

has the potential to treat both primary liver tumors and liver metastases. To this day, transcutaneous ultrasound imaging is the standard modality when treating primary liver tumors using RFA. On the other hand, MRI and CT-scans are the gold standard for imaging liver metastases (Fowler, et al. 2013) since some of them may not be visible when using ultrasound imaging (Kingham, et al. 2018). Ultrasound-guided HIFU treatments is therefore considered only for patients having visible tumors with ultrasound imaging alone (Tonguc, et al. 2021). Moreover, higher visibility of liver metastases was reported when using fusion imaging with ultrasound and MRI which can increase the number of patients that can be treated with ultrasound-guided HIFU (Yee, et al. 2021). Nevertheless, actual grayscale changes on sonograms caused by thermal ablation is already used as an indication of ablation following each sonication (Ji, et al. 2020, Gu, et al. 2021). In our proof of concept study, we have shown that transcutaneous ultrasound imaging provides a reliable evaluation of the treatment after each sonication (R^2=0.84). Each lesion induced by HIFU is visible with high contrast on sonograms. Intraoperative measurements were performed to obtain additional ultrasound imaging measurements under more favorable conditions. As expected, the correlation between dimensions measured on sonograms and gross pathology was higher for intraoperative measurements (R^2=0.92) than transcutaneous measurements (R^2=0.84). Nevertheless, the correlation for transcutaneous measurements was considered as sufficiently high to be a reliable measurement of the HIFU lesions. We found a close correlation between the dimensions of the lesions measured on the transcutaneous sonograms and those measured in gross pathology. This represents a major advantage for the improvement of treatment efficacy since the dimensions of the treatment zone can be enlarged by accurately juxtaposing single lesions without leaving any untreated liver in the ablated zone.

The use of an extracorporeal HIFU device is clinically feasible for the treatment of liver tumors (Leslie, et al. 2012, Yang, et al. 2021), but only a small part (approximately 30%)

of the liver is accessible using a noninvasive HIFU device. In addition, attenuation, phase aberration and liver movements can produce secondary lesions (such as skin burns or gastric lesions) if a completely extracorporeal treatment is performed in the liver. Therefore, the device described in this study was used with animals positioned in a dorsal decubitus proclive position with an angle of 15° to have anatomical access to approximately 60% of the liver while avoiding the rib cage. Under these conditions, ultrasound wave propagation was not impaired by the rib cage. A preliminary evaluation was performed in two patients with hepatic metastases on preoperative CT-scans; where patients had placed their arms above their head. Under these conditions, 3D segmentations showed that this specific positioning of the body creates an acoustic window of approximately 50% of the hepatic volume as it raises the position of the patient's rib cage. For animal experiments, inclination of the surgical table, in addition to strapping the animals' paws above their head, was necessary to obtain a similar accessible volume.

The measured acoustic properties of tissues reported in this study were consistent with those previously reported (Duck 1990). The highest range of these parameters was found for fat tissues ranging from 0.37 $dB.cm^{-1}.MHz^{-1}$ to 1.70 $dB.cm^{-1}.MHz^{-1}$. Such differences in reported data can be the result of measurements performed on fat tissue samples harvested from either the backfat or subcutaneous layers at different parts of the pig's body. Indeed, Gammel and al (Gammell, et al. 1979), reported significant differences in pigs backfat attenuation for studies 23 years apart. They suggested that the feeding and environment of the pigs significantly changed and could therefore have an impact on the acoustic properties of the pigs' tissue. As a result, fat attenuation values can significantly vary depending on the environment and the feeding of the animals. This observation supports the need for individual attenuation measurements in an effort to personalize HIFU treatment. Therefore, attenuation measurements were performed on the pig model that was used in this study. Those

preliminary measurements of the tissue attenuation and *in situ* measurement of the different tissue thicknesses allowed for proper energy deposition at the focus. Moreover, the use of a toroidal transducer allowed for large and fast tissue ablation. Ablations of 21 mm long by 14 mm wide were performed in 40 seconds, allowing the device to be used by hand and under apnea to avoid the deleterious effects of liver movements.

Since this probe was initially designed for intraoperative use, the frequency (2.5 MHz) and the focal length (70 mm) should be changed for the next generation of transducer dedicated for clinical use. A lower frequency and higher focal distance will be used for developing a toroidal HIFU transducer dedicated for extracorporeal application. However, even with a suboptimal transducer, we showed in this study that it was possible to create ablations similar in size and in the time needed than the ones created intraoperatively (Melodelima, et al. 2009, Dupre, et al. 2015). A more optimal device should increase the size of the ablation to treat tumors up to 3 cm in diameter.

The preclinical study described in this article was performed on pigs due to their similar size and physiology to humans. There is no established liver tumor model available in pigs to evaluate HIFU treatments on tumors at the preclinical stage. However, the efficacy of HIFU on liver tumors has been demonstrated in many studies (Battais, et al. 2020, Ji, et al. 2020, Gu, et al. 2021). In addition, anatomopathological studies showed that the lesions created in our experiments were homogeneous. The ability of this toroidal HIFU transducer to create large lesions over short periods of time that are visible with high contrast in real-time on sonograms represents a powerful technique for treating liver tumors noninvasively. The probe can be held by hand, making the device easy to use. As shown on gross pathology and histologic studies, the lesions were homogeneous. There was no untreated liver in the ablated zone, including areas in the vicinity of blood vessels with a diameter up to 5 mm. This should make the treatment of some juxta-vascular tumors possible. The use of such a device can

increase the number of patients eligible for treatment with curative intent by treating tumors that are inaccessible to surgery or other local ablative technologies.

In conclusion, the data presented here suggest that toroidal HIFU transducers are a promising technique for large thermal ablations created noninvasively in the liver. Large and irreversible coagulated volumes can be obtained in short times using this new HIFU device. The ability to produce these noninvasive thermal lesions in the liver, which are visible in real-time and with high contrast on sonograms, may be useful for treating patients with liver tumors.

ACKNOWLEDGMENTS

The authors thank the staff of the Laboratory for Experimental Surgery for their assistance with the animal study. This work was performed within the framework of the SIRIC LyriCAN grant INCa_INSERM_DGOS_12563 and the French National Research Agency (ANR-19-CE19-0027-01).

REFERENCES

Aubry J-F, Pauly KB, Moonen C, Haar G, Ries M, Salomir R, Sokka S, Sekins KM, Shapira Y, Ye F, Huff-Simonin H, Eames M, Hananel A, Kassell N, Napoli A, Hwang JH, Wu F, Zhang L, Melzer A, Kim Y-s, Gedroyc WM. The road to clinical use of high-intensity focused ultrasound for liver cancer: technical and clinical consensus. Journal of Therapeutic Ultrasound 2013;1:13.

Bai Y, Luo X, Li Q, Yin N, Fu X, Zhang H, Qi H. High-intensity focused ultrasound treatment of placenta accreta after vaginal delivery: a preliminary study. Ultrasound Obstet Gynecol 2016;47:492-8.

Barrere V, Sanchez M, Cambronero S, Dupre A, Rivoire M, Melodelima D. Evaluation of Ultrasonic Attenuation in Primary and Secondary Human Liver Tumors and Its Potential Effect on High-Intensity Focused Ultrasound Treatment. Ultrasound Med Biol 2021;47:1761-74.

Battais A, Barrere V, N'Djin WA, Dupre A, Rivoire M, Melodelima D. Fast and Selective Ablation of Liver Tumors by High-Intensity Focused Ultrasound Using a Toroidal Transducer Guided by Ultrasound Imaging: The Results of Animal Experiments. Ultrasound Med Biol 2020;46:3286-95.

Bray F, Ferlay J, Soerjomataram I, Siegel RL, Torre LA, Jemal A. Global cancer statistics 2018: GLOBOCAN estimates of incidence and mortality worldwide for 36 cancers in 185 countries. CA Cancer J Clin 2018;68:394-424.

Caloone J, Huissoud C, Vincenot J, Kocot A, Dehay C, Chapelon JY, Rudigoz RC, Melodelima D. High-intensity focused ultrasound applied to the placenta using a toroidal transducer: a preliminary ex-vivo study. Ultrasound Obstet Gynecol 2015;45:313-9.

Cambronero S, Dupré A, Chen Y, Rivoire PM, Melodelima D. 2020 Intra-operative HIFU treatment at the hepato-caval confluence of the liver in an in vivo porcine model. *2020 IEEE International Ultrasonics Symposium (IUS)*, 1-4.

Cilleros C, Dupre A, Chen Y, Vincenot J, Rivoire M, Melodelima D. Intraoperative HIFU Ablation of the Pancreas Using a Toroidal Transducer in a Porcine Model. The First Step towards a Clinical Treatment of Locally Advanced Pancreatic Cancer. Cancers (Basel) 2021;13.

Crouzet S, Blana A, Murat FJ, Pasticier G, Brown SCW, Conti GN, Ganzer R, Chapet O, Gelet A, Chaussy CG, Robertson CN, Thuroff S, Ward JF. Salvage high-intensity focused ultrasound (HIFU) for locally recurrent prostate cancer after failed radiation therapy: Multi-institutional analysis of 418 patients. BJU Int 2017;119:896-904.

de Senneville BD, Moonen C, Ries M. MRI-Guided HIFU Methods for the Ablation of Liver and Renal Cancers. Adv Exp Med Biol 2016;880:43-63.

Duck FA. Physical Properties of Tissue: Academic Press, 1990.

Dupre A, Melodelima D, Perol D, Chen Y, Vincenot J, Chapelon JY, Rivoire M. First clinical experience of intra-operative high intensity focused ultrasound in patients with colorectal liver metastases: a phase I-IIa study. PLoS One 2015;10:e0118212.

Dupre A, Melodelima D, Perol D, Chen Y, Vincenot J, Chapelon JY, Rivoire M. Evaluation of the Feasibility, Safety, and Accuracy of an Intraoperative High-intensity Focused Ultrasound Device for Treating Liver Metastases. J Vis Exp 2019.

Dupre A, Melodelima D, Pflieger H, Chen Y, Vincenot J, Kocot A, Langonnet S, Rivoire M. Thermal Ablation of the Pancreas With Intraoperative High-Intensity Focused Ultrasound: Safety and Efficacy in a Porcine Model. Pancreas 2017;46:219-24.

Evrard S, Torzilli G, Caballero C, Bonhomme B. Parenchymal sparing surgery brings treatment of colorectal liver metastases into the precision medicine era. Eur J Cancer 2018;104:195-200.

Fowler KJ, Linehan DC, Menias CO. Colorectal liver metastases: state of the art imaging. Ann Surg Oncol 2013;20:1185-93.

Gammell PM, Le Croissette DH, Heyser RC. Temperature and frequency dependence of ultrasonic attenuation in selected tissues. Ultrasound in Medicine & Biology 1979;5:269-77.

Gu L, Shen Z, Ji L, Ng DM, Du N, He N, Fan X, Yan K, Zheng Z, Chen B, Ma L, Qiu G, Chen P, Zheng J, Yang T. High-intensity focused ultrasound alone or combined with transcatheter arterial chemoembolization for the treatment of hepatocellular carcinoma with unsuitable

indications for hepatectomy and radiofrequency ablation: a phase II clinical trial. Surg Endosc 2021.
Haar GT, Coussios C. High intensity focused ultrasound: physical principles and devices. Int J Hyperthermia 2007;23:89-104.
Ji Y, Zhu J, Zhu L, Zhu Y, Zhao H. High-Intensity Focused Ultrasound Ablation for Unresectable Primary and Metastatic Liver Cancer: Real-World Research in a Chinese Tertiary Center With 275 Cases. Front Oncol 2020;10:519164.
Jung SE, Cho SH, Jang JH, Han J-Y. High-intensity focused ultrasound ablation in hepatic and pancreatic cancer: complications. Abdominal Imaging 2011;36:185-95.
Kennedy JE. High-intensity focused ultrasound in the treatment of solid tumours. Nature Reviews Cancer 2005;5:321-27.
Kennedy JE, Wu F, ter Haar GR, Gleeson FV, Phillips RR, Middleton MR, Cranston D. High-intensity focused ultrasound for the treatment of liver tumours. Ultrasonics 2004;42:931-35.
Kingham TP, Pak LM, Simpson AL, Leung U, Doussot A, D'Angelica MI, DeMatteo RP, Allen PJ, Jarnagin WR. 3D image guidance assisted identification of colorectal cancer liver metastases not seen on intraoperative ultrasound: results from a prospective trial. HPB (Oxford) 2018;20:260-67.
Lang BH, Wu ALH. High intensity focused ultrasound (HIFU) ablation of benign thyroid nodules - a systematic review. J Ther Ultrasound 2017;5:11.
Leslie T, Ritchie R, Illing R, Ter Haar G, Phillips R, Middleton M, Bch B, Wu F, Cranston D. High-intensity focused ultrasound treatment of liver tumours: post-treatment MRI correlates well with intra-operative estimates of treatment volume. Br J Radiol 2012;85:1363-70.
Lesser TG, Boltze C, Schubert H, Wolfram F. Flooded Lung Generates a Suitable Acoustic Pathway for Transthoracic Application of High Intensity Focused Ultrasound in Liver. Int J Med Sci 2016;13:741-48.
Maloney E, Hwang JH. Emerging HIFU applications in cancer therapy. Int J Hyperthermia 2015;31:302-9.
Melodelima D, N'Djin WA, Favre-Cabrera J, Parmentier H, Rivoire M, Chapelon JY. Thermal ablation produced using a surgical toroidal high-intensity focused ultrasound device is independent from hepatic inflow occlusion. Physics in medicine and biology 2009;54:6353-68.
Melodelima D, N'Djin WA, Favre-Cabrera J, Parmentier H, Rivoire M, Chapelon JY. Thermal ablation produced using a surgical toroidal high-intensity focused ultrasound device is independent from hepatic inflow occlusion. Phys Med Biol 2009;54:6353-68.
Melodelima D, N'Djin WA, Parmentier H, Chesnais S, Rivoire M, Chapelon JY. Thermal ablation by high-intensity-focused ultrasound using a toroid transducer increases the coagulated volume. Results of animal experiments. Ultrasound Med Biol 2009;35:425-35.
Melodelima D, N'Djin WA, Parmentier H, Chesnais S, Rivoire M, Chapelon J-Y. Ultrasound surgery with a toric transducer allows the treatment of large volumes over short periods of time. Applied Physics Letters 2007;91:193901.
Melodelima D, Prat F, Fritsch J, Theillere Y, Cathignol D. Treatment of esophageal tumors using high intensity intraluminal ultrasound: first clinical results. J Transl Med 2008;6:28.
Melodelima D, Salomir R, Chapelon JY, Theillere Y, Moonen C, Cathignol D. Intraluminal high intensity ultrasound treatment in the esophagus under fast MR temperature mapping: in vivo studies. Magn Reson Med 2005;54:975-82.
N'Djin WA, Chapelon JY, Melodelima D. An Ultrasound Image-Based Dynamic Fusion Modeling Method for Predicting the Quantitative Impact of In Vivo Liver Motion on Intraoperative HIFU Therapies: Investigations in a Porcine Model. PLoS One 2015;10:e0137317.
N'Djin WA, Melodelima D, Parmentier H, Rivoire M, Chapelon JY. In vivo preclinical evaluation of the accuracy of toroidal-shaped HIFU treatments using a tumor-mimic model. Phys Med Biol 2010;55:2137-54.
Nordlinger B, Sorbye H, Glimelius B, Poston GJ, Schlag PM, Rougier P, Bechstein WO, Primrose JN, Walpole ET, Finch-Jones M, Jaeck D, Mirza D, Parks RW, Mauer M, Tanis E, Van Cutsem E, Scheithauer W, Gruenberger T. Perioperative FOLFOX4 chemotherapy and surgery versus

surgery alone for resectable liver metastases from colorectal cancer (EORTC 40983): long-term results of a randomised, controlled, phase 3 trial. The Lancet Oncology 2013;14:1208-15.
Parmentier H, Melodelima D, N'Djin A, Chesnais S, Chapelon JY, Rivoire M. High-intensity focused ultrasound ablation for the treatment of colorectal liver metastases during an open procedure: study on the pig. Ann Surg 2009;249:129-36.
Sanchez M, Barrere V, Treilleux I, Chopin N, Melodelima D. Development of a noninvasive HIFU treatment for breast adenocarcinomas using a toroidal transducer based on preliminary attenuation measurements. Ultrasonics 2021;115:106459.
Sehmbi AS, Froghi S, Oliveira de Andrade M, Saffari N, Fuller B, Quaglia A, Davidson B. Systematic review of the role of high intensity focused ultrasound (HIFU) in treating malignant lesions of the hepatobiliary system. HPB (Oxford) 2021;23:187-96.
Siedek F, Yeo SY, Heijman E, Grinstein O, Bratke G, Heneweer C, Puesken M, Persigehl T, Maintz D, Grull H. Magnetic Resonance-Guided High-Intensity Focused Ultrasound (MR-HIFU): Technical Background and Overview of Current Clinical Applications (Part 1). Rofo 2019;191:522-30.
Sung H, Ferlay J, Siegel RL, Laversanne M, Soerjomataram I, Jemal A, Bray F. Global Cancer Statistics 2020: GLOBOCAN Estimates of Incidence and Mortality Worldwide for 36 Cancers in 185 Countries. CA Cancer J Clin 2021;71:209-49.
Tonguc T, Strunk H, Gonzalez-Carmona MA, Recker F, Lutjohann D, Thudium M, Conrad R, Becher MU, Savchenko O, Davidova D, Luechters G, Mustea A, Strassburg CP, Attenberger U, Pieper CC, Jenne J, Marinova M. US-guided high-intensity focused ultrasound (HIFU) of abdominal tumors: outcome, early ablation-related laboratory changes and inflammatory reaction. A single-center experience from Germany. Int J Hyperthermia 2021;38:65-74.
Yang T, Ng DM, Du N, He N, Dai X, Chen P, Wu F, Chen B, Fan X, Yan K, Zhou X, Dong M, Zheng Z, Gu L. HIFU for the treatment of difficult colorectal liver metastases with unsuitable indications for resection and radiofrequency ablation: a phase I clinical trial. Surg Endosc 2021;35:2306-15.
Yee CH, Chiu PK, Teoh JY, Ng CF, Chan CK, Hou SM. High-Intensity Focused Ultrasound (HIFU) Focal Therapy for Localized Prostate Cancer with MRI-US Fusion Platform. Adv Urol 2021;2021:7157973.

FIGURE CAPTIONS LIST

Figure 1. Front view of the toroidal device with the ultrasound imaging probe integrated at its center.

Figure 2. Toroidal HIFU device in contact with the animal's skin during sonication.

Figure 3: HIFU ablation cut through the middle, near the large vessels. A. Front view, the vessel separated the ablation into two parts. B. Side view of the vessels behind the ablation. C. Intraoperative ultrasound image at D7 of the vessel and HIFU ablation. One of the vessels is clearly passing through the ablated zone. The section of this vessel was 8.7 mm long by 2.4 mm in diameter.

Figure 4: Three HIFU ablations that were compliant. A. Ablation in the liver with an emitted energy of 5560 J in an animal with an abdominal wall thickness of 16.8 mm. B. Ablation in the liver with an emitted energy of 5640 J in an animal with an abdominal wall thickness of 13.3 mm. C. HIFU ablation compliant created around a vessel with a diameter < 5 mm.

Figure 5: Histological results. Microscopic view of the liver tissue showing the separation between the HIFU ablation and the surrounding untreated liver.

Figure 6: Ultrasound images of the HIFU procedure in animals n=13 acquired at D0 before (A) and after HIFU sonications (B) and at D7 before (C) and after (D) laparotomy. The abdominal wall thickness was 13.3 mm. The delivered energy was 5720 J, resulting in ablation in the liver. A hyperechoic zone is observed around the theoretical point of maximum pressure (B, C and D) as well as a surrounding hypoechoic region. (D) At Day 7, a hyperechoic boundary was observed all around the ablation intraoperatively.

Figure 7: Correlation between dimensions measured on sonograms and gross pathology using intraoperative (left) or transcutaneous measurements at Day 7. White dots indicate the

measurements of the long axis, and black dots indicate measurements of the short axis of the HIFU ablations.

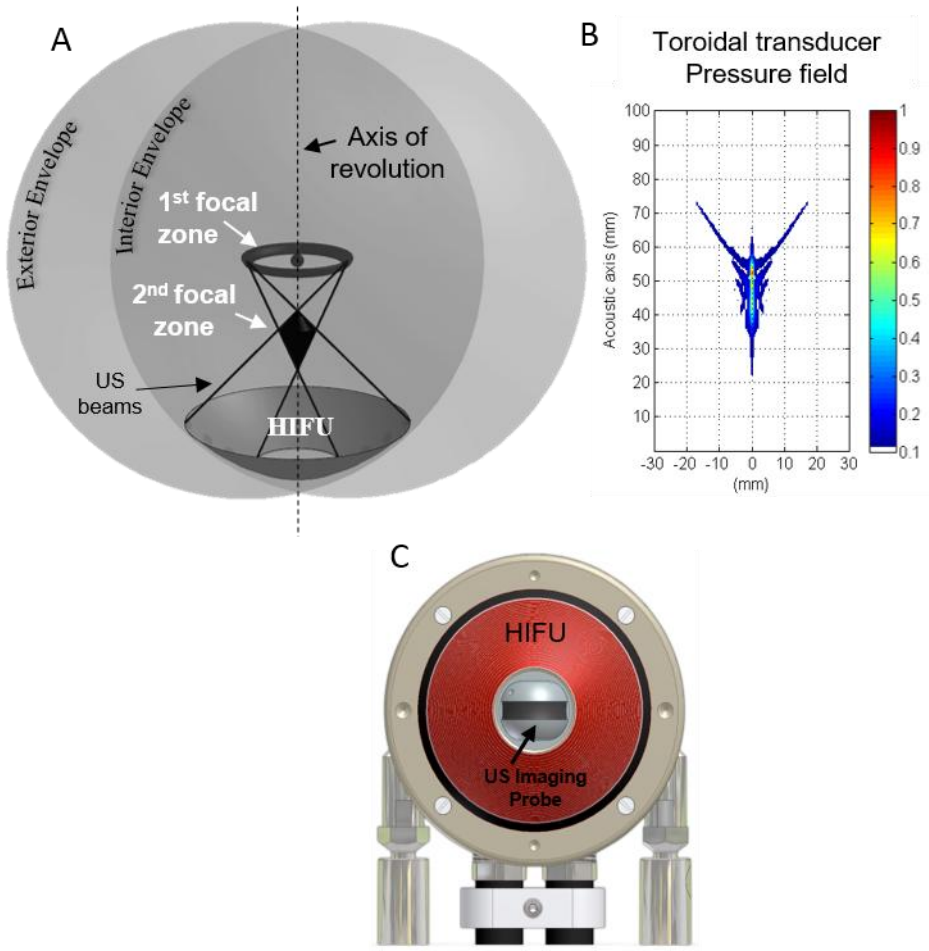

Figure 1. Toroidal transducer and its natural focusing. A, 3D geometric view of the toroidal geometry. The toroidal transducer is built on a portion of the interior envelope. The transducer has two focal zones: a ring and a kite-shaped zone. B, Pressure field of the natural focusing of the toroidal probe. The pressure at the second focal zone is, in general, higher than the pressure at the ring. Therefore, the kite-shaped zone is mainly used for treatments. C, Front view of the toroidal device with the ultrasound imaging probe integrated at its center.

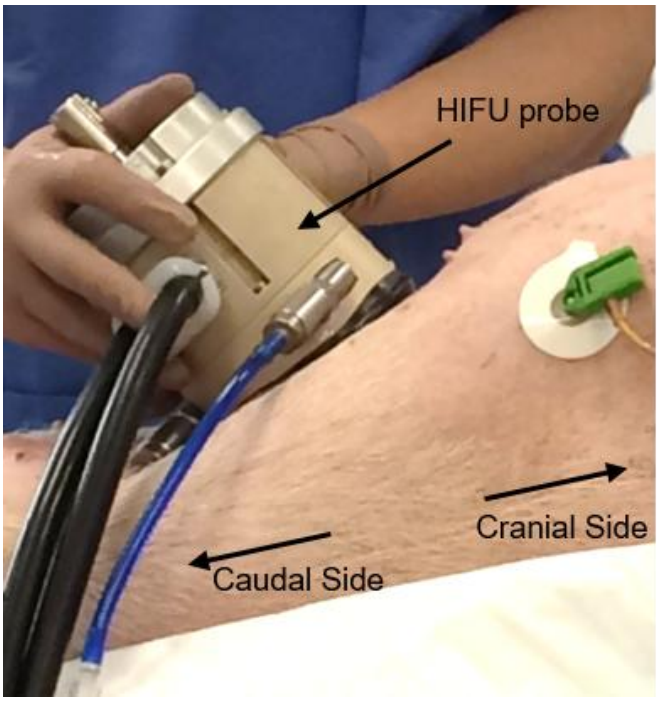

Figure 2. Toroidal HIFU device in contact with the animal's skin during sonication.

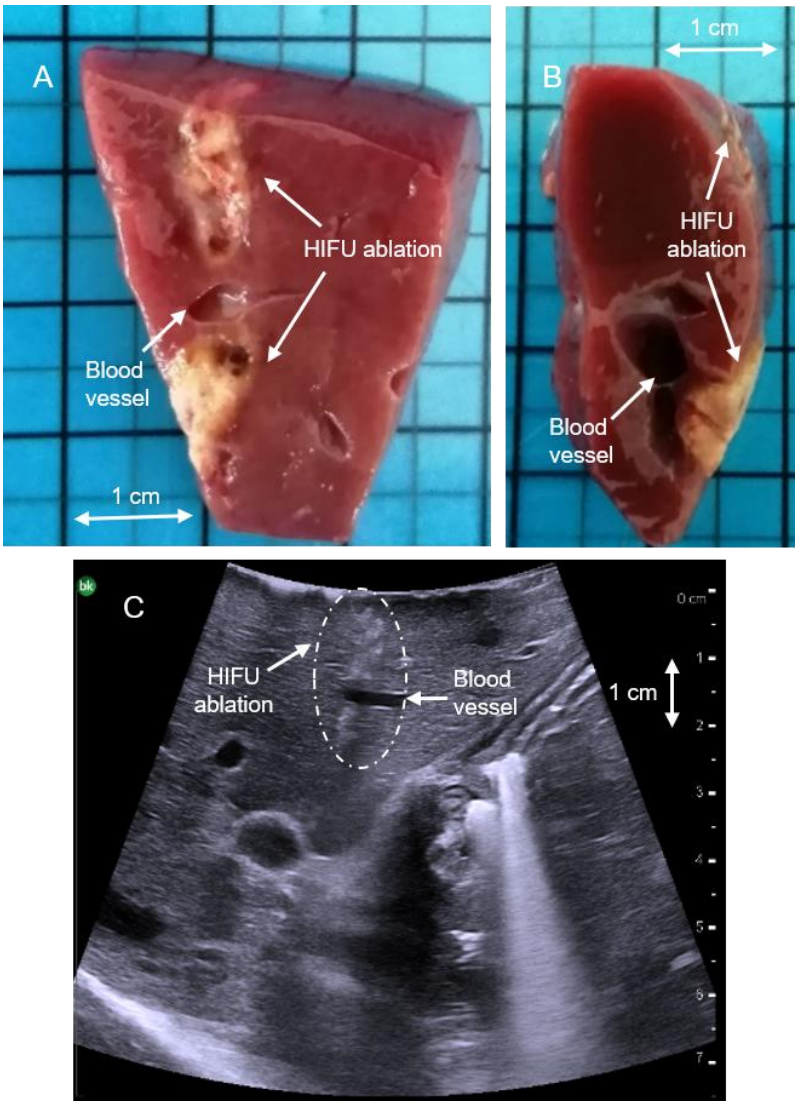

Figure 3: HIFU ablation cut through the middle, near the large vessels. A. Front view, the vessel separated the ablation into two parts. The bottom left part of the HIFU ablation was removed in the perpendicular plane in an effort to reveal the vessel on the side view. B. Side view of the vessels behind the ablation. C. Intraoperative ultrasound image at D7 of the vessel and HIFU ablation. One of the vessels is clearly passing through the ablated zone. The section of this vessel was 8.7 mm long by 2.4 mm in diameter.

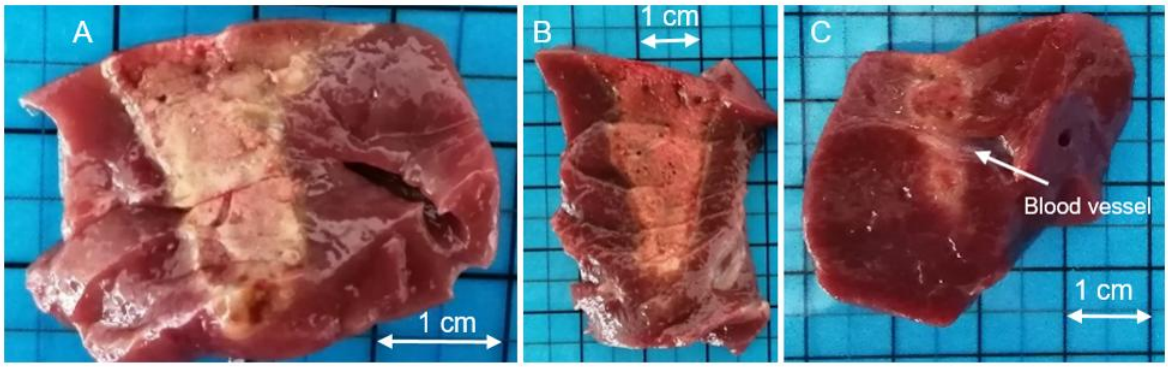

Figure 4: Three HIFU ablations that were compliant. A. Ablation in the liver with an emitted energy of 5560 J in an animal with an abdominal wall thickness of 16.8 mm. B. Ablation in the liver with an emitted energy of 5640 J in an animal with an abdominal wall thickness of 13.3 mm. C. HIFU ablation compliant created around a vessel with a diameter < 5 mm.

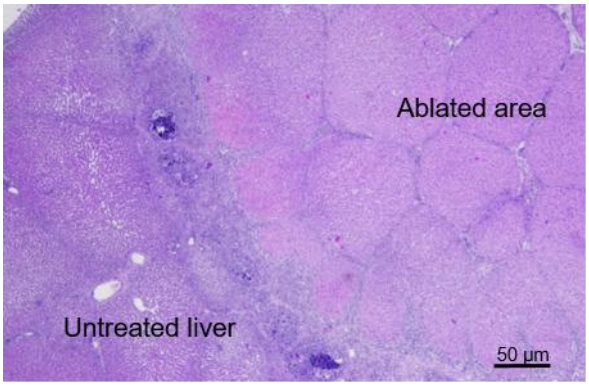

Figure 5: Histological results. Microscopic view of the liver tissue showing the separation between the HIFU ablation and the surrounding untreated liver.

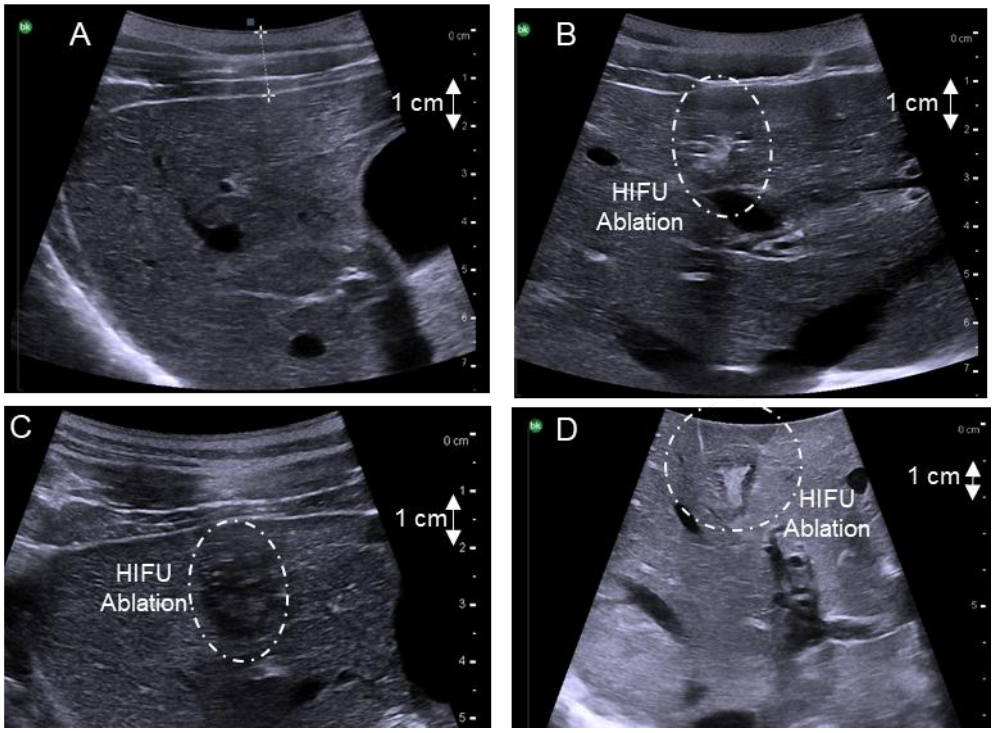

Figure 6: Ultrasound images of the HIFU procedure in animals n=13 acquired at D0 before (A) and after HIFU sonications (B) and at D7 before (C) and after (D) laparotomy. The abdominal wall thickness was 13.3 mm at D0 and 14.7 mm at D7. The delivered energy was 5720 J, resulting in ablation in the liver. A hyperechoic zone is observed around the theoretical point of maximum pressure (B, C and D) as well as a surrounding hypoechoic region. (D) At Day 7, a hyperechoic boundary was observed all around the ablation intraoperatively.

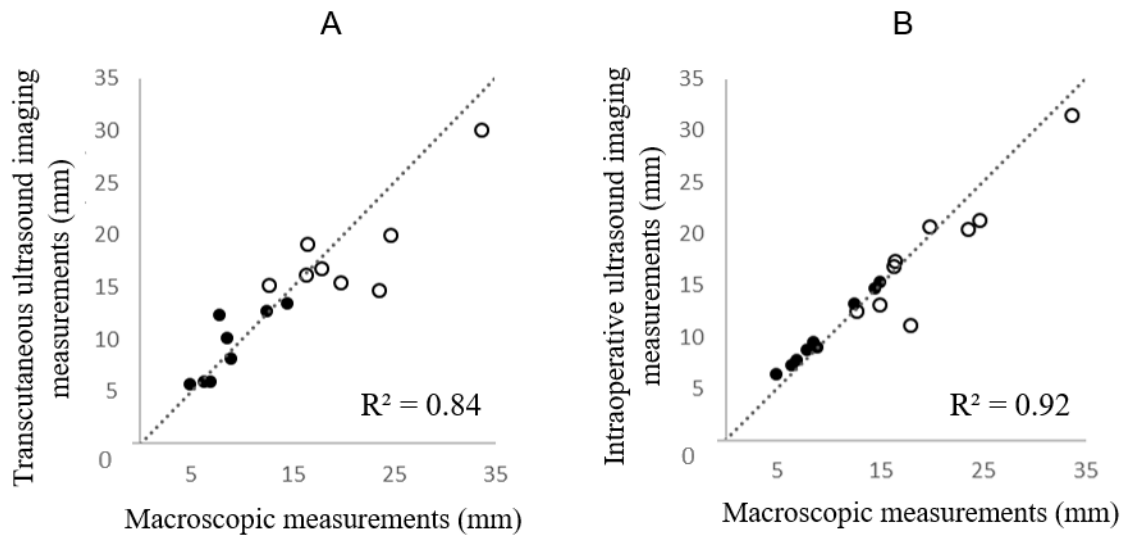

Figure 7: Correlation between dimensions measured on sonograms and gross pathology. (a) transcutaneous (with intact layered tissue) imaging and (b) intraoperative imaging. Both measurements were performed at Day 7. White dots indicate the measurements of the long axis, and black dots indicate measurements of the short axis of the HIFU ablations.

Sonication number	Thickness from skin to focus (mm)	Tissue attenuation (dB)	$E_{applied}$ (J)	$E_{delivered}$ (J)	$P_{applied}$ (W)	$P_{delivered}$ (W)	T/NT/TNC
1	35.5	4.3	4600	1651	115	41	NT
2	34.5	4.5	4560	1574	114	39	NT
3	36.0	4.3	5600	1997	140	50	TNC
4	36.8	4.3	5600	1997	140	50	T
5	35.4	4.4	5520	1920	138	48	TNC
6	35.6	4.0	5560	2112	139	53	T
7	36.0	4.5	5640	1920	141	48	T
8	35.6	4.1	5680	2112	142	53	TNC
9	36.6	4.4	5600	1958	140	49	T
10	36.8	4.6	5760	1920	144	48	T
11	35.8	4.3	5640	2035	141	51	T
12	36.3	4.2	5640	2074	141	52	T
13	35.8	4.6	5720	1920	143	48	T
14	36.6	4.5	5600	1882	140	47	T

Table 1. Treatment results overview. Attenuation from the skin to the focus was computed using Equation 5 based on acoustic characterization of porcine tissues and on the measured abdominal wall thickness just before sonication. The applied acoustic power was computed from the measurement of the electrical power during sonication, considering the efficiency of the transducer (60%). The delivered acoustic power was computed from Equation 4. NT: Not Treated (no visible damage), T: Treated (Visible damage at the target site compliant with the planned lesion size), TNC: Treated but not compliant (visible damage at the target site but not compliant with the planned lesion size).

Tissue	Coefficient a (dB.cm-1.MHz-1)	Coefficient b	Density ($Kg.m^{-3}$)	Speed of sound ($m.s^{-1}$)	Transmission coefficients
Skin	1.56 ± 0.43	1.19 ± 0.06	1104 ± 39	1555 ± 52	0.99
Fat	0.43 ± 0.09	1.39 ± 0.01	990 ± 98	1465 ± 37	0.99
Muscle	0.78 ± 0.26	1.70 ± 0.07	1111 ± 64	1566 ± 11	0.99
Liver	0.61 ± 0.17	1.30 ± 0.03	1048 ± 80	1537 ± 61	0.99

Table 2. Measured tissues properties: attenuation coefficients that varied with frequency as $\alpha = af^b$, density, speed of sound and transmission coefficients at the water/skin, skin/fat, fat/muscle, muscle/liver interfaces. The total transmission coefficient T was defined as the product of all the transmission coefficients listed in the table, T=0.96.